Chinese Journal of
POLYMER SCIENCE

RESEARCH ARTICLE

https://doi.org/10.1007/s10118-026-3897-x
Chinese J. Polym. Sci.

Multifunctional Oligomer as Fluorine-free Flame-retardant Additive of Liquid Electrolytes Enables Simultaneously High Safety and Long-cycle Life in Lithium-ion Batteries

Xing-Di Li[a,†], Yi-Zhou Quan[b,†], Ji-Yun Ma[a], and Gang Wu[a*]

[a] *Collaborative Innovation Center for Eco-Friendly and Fire-Safety Polymeric Materials (MoE), National Engineering Laboratory of Eco-Friendly Polymeric Materials (Sichuan), State Key Laboratory of Advanced Polymeric Materials, College of Chemistry, Sichuan University, Chengdu 610064, China*
[b] *Dongfang Electric (Chengdu) Hydrogen Technology Limited, Chengdu 611731, China*

Electronic Supplementary Information

Abstract Lithium-ion batteries (LIBs) face significant thermal runaway challenges because of the flammability of commercial organic liquid electrolytes. Therefore, the development of flame-retardant liquid electrolytes is essential to enhance intrinsic safety. In this study, a fluorine-free poly(phenoxyphosphonate-ethylene glycol) oligomer (PBO) was synthesized as a novel multifunctional flame-retardant additive for liquid electrolytes. By incorporating thermally stable phenoxyphosphonate structures and electrode-compatible poly(ethylene glycol) (PEG) segments, PBO improved the thermal stability of the liquid electrolyte and suppressed gas generation. Experimental results demonstrate that PBO outperforms the commercial flame retardant ethoxy(pentafluoro)cyclotriphosphazene (PFPN) in enhancing the thermal runaway resistance. Specifically, coin cells using the BE-15% PBO liquid electrolyte (where BE denotes blank electrolyte, *i.e.* commercial electrolyte, 1 mol·L^{-1} $LiPF_6$ in ethylene carbonate/dimethyl carbonate/ethyl methyl carbonate, *V*/*V*/*V*=1/1/1) exhibit 84.9% capacity retention after 300 cycles at 1.0 C. Furthermore, 1 Ah pouch cells maintain 847.9 mAh after 250 cycles at 0.5 C and achieve 95.1% retention after 200 cycles at 1.0 C. These superior properties are attributed to the inhibition of combustion chain reactions by the phosphorus-containing radicals generated during PBO decomposition and the formation of a stable interfacial layer on the graphite anode.

Keywords Lithium-ion battery; Flame-retardant additive; Oligomer; Thermal/fire safety; Long-cycle life

Citation: Li, X. D.; Quan, Y. Z.; Ma, J. Y.; Wu, G. Multifunctional oligomer as fluorine-free flame-retardant additive of liquid electrolytes enables simultaneously high safety and long-cycle life in lithium-ion batteries. *Chinese J. Polym. Sci.* https://doi.org/10.1007/s10118-026-3897-x

INTRODUCTION

Lithium-ion batteries (LIBs) have emerged as the most promising energy-storage technology owing to their high energy density and long cycle life. However, their inherent safety hazard, the risk of thermal runaway (TR), severely restricts their commercialization.[1–4] Commercial LIBs use liquid electrolytes based on flammable organic solvents, which can easily catch fires or explosions under abuse conditions. Therefore, the development of flame-retardant liquid electrolytes is crucial to enhance the inherent safety of LIBs.[5–7]

In recent years, significant progress has been made in the research of flame-retardant liquid electrolytes, with the main strategies including flame-retardant additives, co-solvents, high-concentration electrolytes, and gel polymer electrolytes.[8] Among these, the direct addition of flame retardants to commercial liquid electrolytes is the mainstream strategy because of its simple operation and ease of industrialization.[9] Traditional small-molecule phosphorus-containing flame retardants, such as trimethyl phosphate (TMP),[10] triethyl phosphate (TEP),[11] dimethyl methanephosphonate (DMMP),[12] and triphenyl phosphate (TPP),[13] achieve efficient flame retardancy through the gas-phase free-radical trapping mechanism, but they generally have poor compatibility with graphite anodes. Furthermore, even at low addition levels, battery cycle performance can be severely degraded, limiting their practical application in high-performance LIBs.[14,15]

In response to the limitations of traditional flame retardants, researchers have made numerous efforts, such as introducing fluorine-containing flame-retardant additives, fluorine-containing solvents, liquid polymer electrolytes, and high-concentration lithium salts to enhance the fire safety of LIBs.[16–18] These methods aim to improve the electrochemical stability of flame-retardant liquid electrolytes and optimize battery performance by forming a stable solid elec-

* Corresponding author, E-mail: gangwu@scu.edu.cn
† These authors contributed equally to this work.
Invited Research Article
Received August 12, 2026; Accepted September 17, 2026; Published online November 23, 2026

© Chinese Chemical Society
Institute of Chemistry, Chinese Academy of Sciences

trolyte interphase (SEI) layer on the surface of the electrode.[19,20] However, the preparation of these additives, solvents, and flame-retardant liquid electrolytes often involves complex processes and synthesis methods, and they also face a series of problems, such as high raw material costs and environmental unfriendliness, which significantly increases the difficulty of their commercial application.[21,22] Therefore, developing new flame-retardant additives that are low-cost, easy to prepare, and possess efficient flame retardancy, electrode compatibility, and electrochemical stability is of great significance for safe LIBs.[23,24]

Ethoxy(pentafluoro)cyclotriphosphazene (PFPN) is one of the most promising multifunctional liquid electrolyte additives. It possesses both flame retardancy and interface optimization advantages, but it has a high viscosity and high cost, and usually needs to be used in combination.[25,26] Inspired by solid-state polymer electrolytes, fluorine-free phosphorus-containing oligomers have been used as liquid electrolytes.[27,28] For instance, the phosphonate-containing poly(ethylene glycol) (PEG)-based oligomer (PPO) designed by Quan *et al*. not only provides a liquid electrolyte with good flame retardancy, fluidity, and high ionic conductivity, but also fails to completely prevent combustion and lacks application and safety evaluation in pouch batteries.[29]

Given that the thermal runaway of LIBs is mainly caused by abnormal temperature increases under abusive conditions, leading to an internal chain reaction, and that during charging and discharging, the electrolyte continuously decomposes on the surface of the graphite anode to form an SEI layer accompanied by the generation of a large amount of gas, which causes an increase in internal pressure, structural deformation, and internal short circuits in pouch batteries, ultimately leading to thermal runaway.[30,31]

In this work, to effectively delay the thermal runaway process and inhibit the decomposition and gas generation of liquid electrolytes, as shown in Fig. 1(a), we rationally designed and successfully synthesized a novel polymer-type flame-retardant additive for a commercial liquid electrolyte, that is, poly(phenoxyphosphonate-ethylene glycol) (PBO) oligomer combining a phenyloxyphosphate structure with a PEG structure, which not only integrates a variety of functions, including flame retardancy, but also plays a synergistic role in the electrochemical performance of liquid electrolytes. Compared with the commercially promising PFPN, PBO can more effectively enhance the thermal stability of the liquid electrolyte at high temperatures, significantly inhibiting its decomposition and the release of both heat and gas, while delivering excellent battery performance (Fig. 1b). The results show that the $LiFePO_4$/graphite (LFP/Gr) coin batteries maintained a capacity retention of 84.9% after 300 cycles at 1.0 C, while the 1 Ah pouch LFP/Gr batteries still had a remaining capacity of 847.9 mAh after 250 cycles at 0.5 C, and the capacity retention was as high as 95.1% after 200 cycles at 1.0 C. These data demonstrate the advantages of the PBO flame retardant in maintaining high electrochemical performance and improving the safety of the battery.

EXPERIMENTAL

The experimental sections are described in the electronic sup-

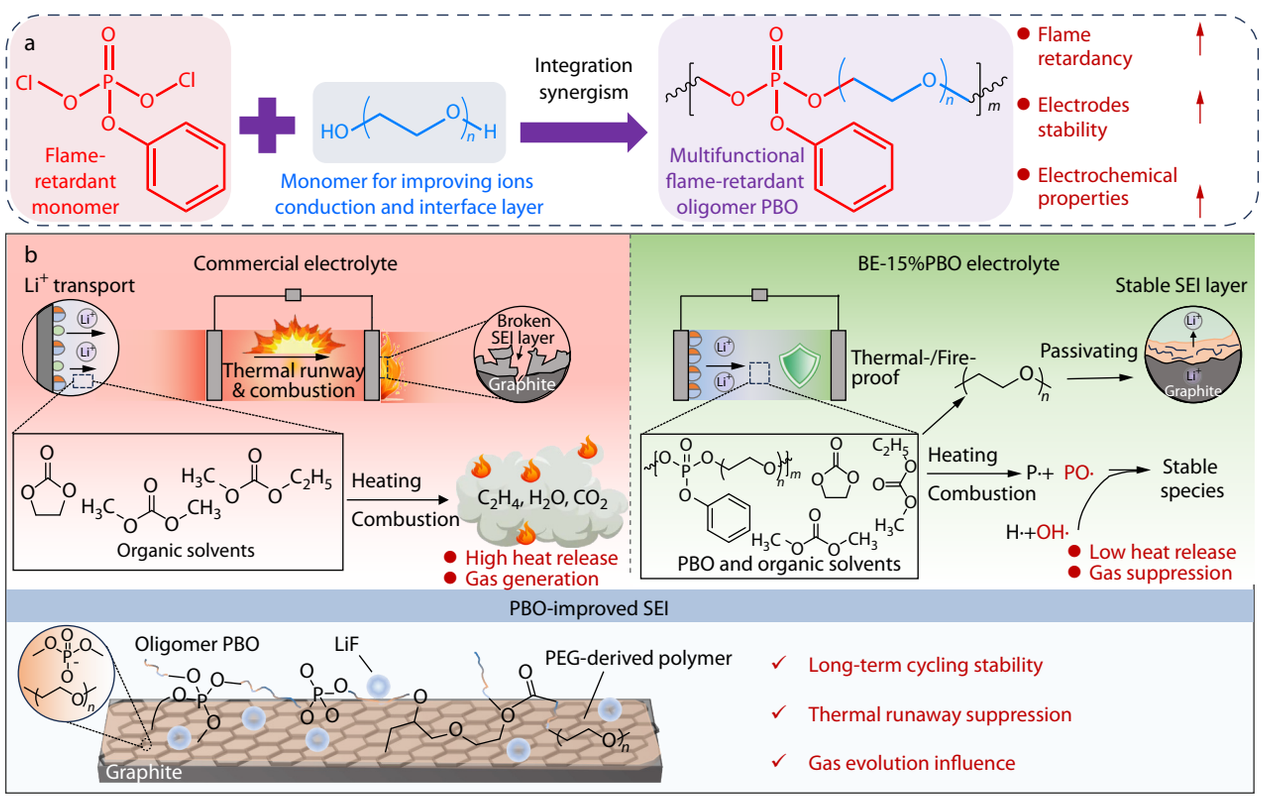


Fig. 1 Schematic illustration of (a) design principle and (b) working mechanism of the oligomer additive (PBO).

https://doi.org/10.1007/s10118-026-3897-x

plementary information (ESI).

RESULTS AND DISCUSSION

Characterization of PBO and Electrolytes

To obtain the additive, PBO was synthesized *via* a one-step process using phenoxyphosphoryl dichloride and PEG. The detailed preparation process is described in ESI. The chemical structure of PBO was characterized by nuclear magnetic resonance (NMR) and gel permeation chromatography (GPC). The obtained PBO was a brown, highly viscous liquid at room temperature (inset of Fig. 2A). In the ^{1}H-NMR spectrum (Fig. 2A), all the main peaks were clearly assigned, and there was only one peak in the ^{31}P-NMR spectrum (Fig. 2B), indicating that the structurally clear PBO oligomer was successfully synthesized. The molar percentage content of the phosphates in PBO was calculated using the ^{1}H-NMR spectrum to be approximately 61%. As shown in Fig. S1 (in ESI), the weight-average molecular weight (M_w) and polydispersity index (M_w/M_n) from the GPC test are 5.15 kDa and 1.36, respectively.

The thermal properties of the PBO were investigated using differential scanning calorimetry (DSC) and thermogravimetric (TG) analysis. The DSC heating curve in Fig. 2(C) shows that the glass transition temperature (T_g) of PBO is only –46.0 °C, suggesting that PBO has good molecular flexibility and strong molecular chain activity, suggesting that the introduction of PBO into liquid electrolytes is beneficial for lithium-ion transport. The TG curve of PBO in Fig. 2(D) shows that the initial decomposition temperature ($T_{5\%}$, the temperature at which 5% weight loss occurs) is 242 °C and the maximum decomposition temperature (T_{max}) is 282 °C, proving that PBO has excellent thermal stability.

The total heat release of the liquid electrolyte from combustion to extinction was measured using a sealed combustion oxygen-consumption testing device (experimental details are available in ESI).[29] The experimental results are presented in Fig. 2(E). The total heat release of the commercial liquid electrolyte (blank electrolyte, BE) during combustion was 832.5 J. However, after introducing 5% PFPN or 15% PBO flame retardants, the total heat release of the liquid electrolyte decreased to 0 J, indicating that these two formulations have excellent fire safety properties. As shown in Fig. 2(F), after continuous ignition for 1 s, the 15% PBO liquid electrolyte (BE-15% PBO) could achieve self-extinguishing after removing the igniter, and it could not be ignited even after the second consecutive ignition. The high-temperature thermal stability of the liquid electrolyte was tested by thermogravimetric analysis (Fig. 2G). The weight loss of the liquid electrolytes mainly occurred in the ranges of 100–150 °C (linear carbonate volatilization) and 200–275 °C (ethylene carbonate volatilization and lithium salt decomposition). The weight loss of BE-15% PBO in the first stage was significantly

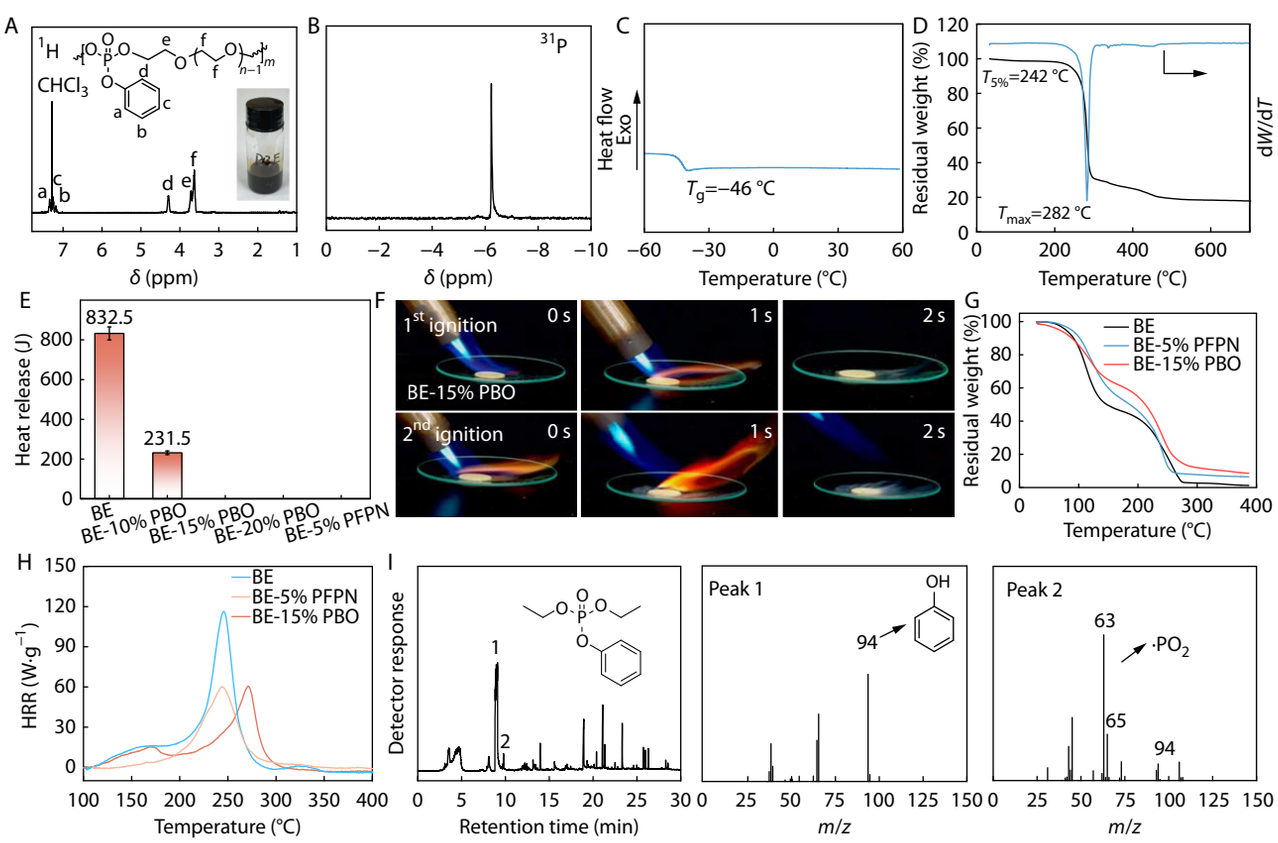


Fig. 2 (A) ^{1}H-NMR and (B) ^{31}P-NMR spectra of PBO; (C) Differential scanning calorimetry curve and (D) thermogravimetric analysis curve of PBO; (E) Test for oxygen consumption during combustion of different liquid electrolytes; (F) Combustion experiments of BE-15% PBO; (G) TG curves of different liquid electrolytes; (H) Heat release rate of different liquid electrolytes; (I) Total ion chromatograms of PBO obtained from the Py-GC-MS test.

https://doi.org/10.1007/s10118-026-3897-x

lower than that of BE; in the 125–275 °C range, the thermal stability of BE-15% PBO was significantly better than that of 5% PFPN liquid electrolyte (BE-5% PFPN) because the small-molecule PFPN is easily volatile. The microcalorimetry (MCC) test (Fig. 2H) further confirmed that PBO not only delayed the peak heat release temperature (T_{HRR}) of the liquid electrolyte from 245.6 °C to 271.3 °C, but also significantly reduced the peak heat release rate (PHRR) and total heat release (THR), similar to PFPN (Table S1 in ESI), indicating that PBO would be effective in weakening the thermal runaway.

In addition, pyrolysis gas chromatography-mass spectrometry (Py-GC-MS) further revealed the detailed decomposition and pyrolysis processes of PBO at 300 °C. As shown in Fig. 2(I), the main decomposition products of PBO are the phenolic structure (m/z=94) at the 1st peak and the ·PO_2 (m/z=63) radical at the 2nd peak, which captures ·H, ·OH, and hydrocarbon radicals during electrolyte combustion, thereby inhibiting the combustion of the liquid electrolyte.[6,32]

Electrochemical Properties and Cells Performance

The influence of different amounts of PBO on the ionic transport ability of the liquid electrolyte was investigated using electrochemical impedance spectroscopy (EIS) (Figs. 3a and 3b). The results show that the impedances of the blank electrolyte (BE), 10% PBO liquid electrolyte (BE-10% PBO), BE-15% PBO, 20% PBO liquid electrolyte (BE-20% PBO), and BE-5% PFPN are 0.83, 1.83, 1.99, 2.51, and 2.21 Ω, respectively, and the corresponding ionic conductivities are 1.35, 0.61, 0.56, 0.45, and 0.51 mS·cm^{-1}. Notably, when the PBO addition amount reaches 15%, its conductivity (0.56 mS·cm^{-1}) is still superior to that of the BE-5% PFPN liquid electrolyte. This is attributed to the unique molecular chain segment movement ability of PBO, which provides an efficient transport channel for Li ions. However, the conductivity of BE-15% PBO is lower than that of BE. This reduction was mainly due to the elevated electrolyte viscosity upon PBO addition, which impeded the rapid migration of Li^+ solvated species and increased the overall bulk resistance. Despite this viscosity-induced conductivity drop, the rapid segmental motion of the PBO chains facilitated localized Li^+ hopping, enabling the BE-15% PBO electrolyte to maintain a fast ionic transport capability that remained superior to that of BE-5% PFPN.[33,34] Meanwhile, the abundant polar functional groups (such as P═O and ether chains) in the PBO structure can effectively modulate the surface wettability, bringing it to a level comparable to that of pristine separator/electrode materials.[35,36] As shown in Fig. S2 (in

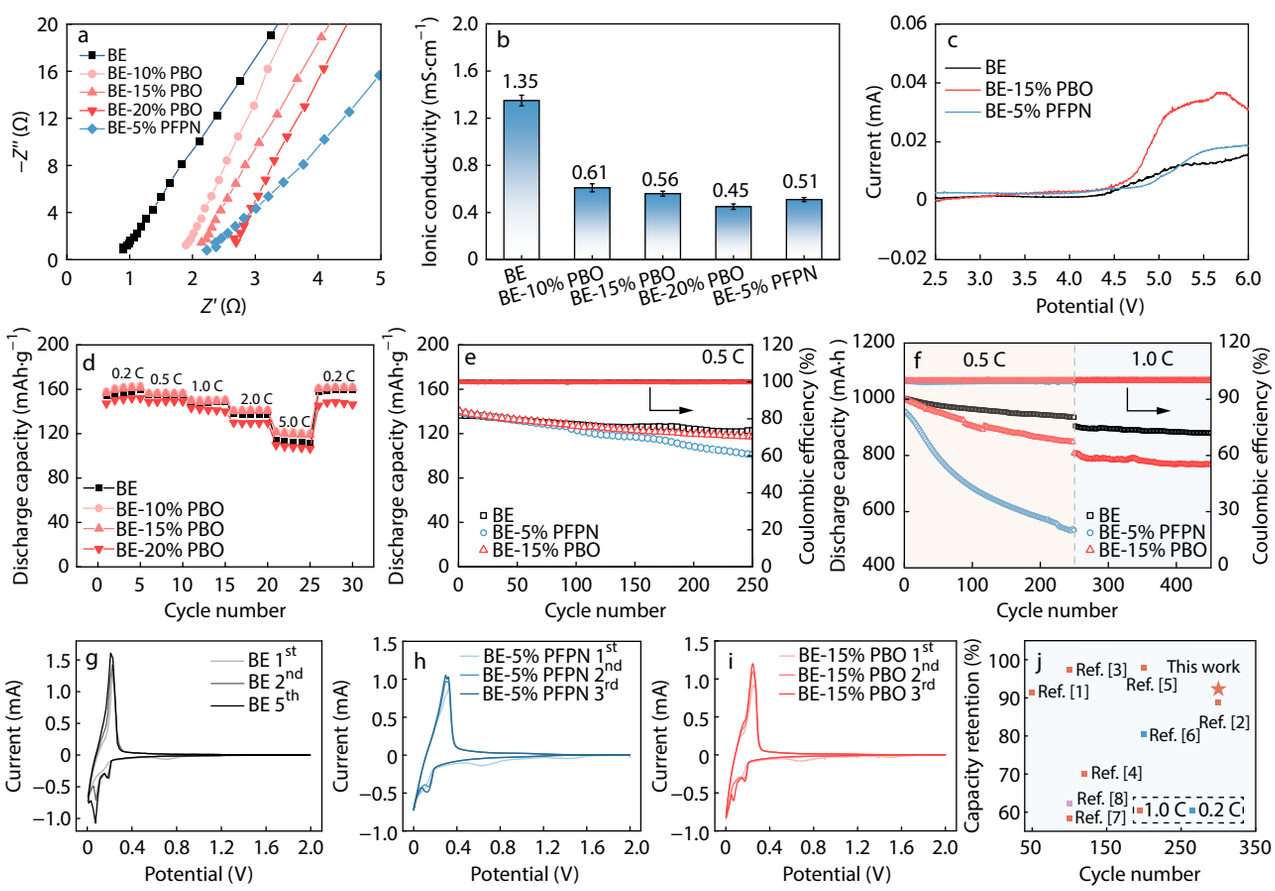


Fig. 3 (a) Electrochemical impedance spectroscopy and (b) ionic conductivity of different liquid electrolytes with PP separator; (c) Linear sweep voltammetry curves for different liquid electrolytes, scan rate = 1 mV·s^{-1}; (d) Rate performance of LFP/Li cells with different liquid electrolytes; (e) Cycling performance of LFP/Gr cells with different liquid electrolytes at the rate of 0.5 C; (f) Cycling performance of the LFP/Gr pouch cells with different liquid electrolytes at 0.5 and 1.0 C; Cyclic voltammetry curves of Gr/Li cells with (g) BE, (h) BE-5% PFPN and (i) BE-15% PBO liquid electrolytes, scan range = 0–2 V, scan rate = 0.1 mV·s^{-1}; (j) Comparison of cycle performance between our work and the reported flame-retardant additives in LIBs (corresponding references can be found in Table S9 in ESI).

https://doi.org/10.1007/s10118-026-3897-x

ESI), the contact angle of BE-15% PBO with the polypropylene (PP) separator is similar to that of BE. Combined with the aforementioned oxygen consumption testing results and ionic conductivity, 15% PBO significantly improved the fire safety of the liquid electrolyte while maximizing the retention of its kinetic performance. Therefore, this study determined that 15% PBO (BE-15% PBO) was the optimal proportion for subsequent experiments.

Subsequently, the oxidation stability of the liquid electrolytes was determined by linear sweep voltammetry (LSV) (Fig. 3c). BE-15% PBO did not produce an obvious oxidation current before 4.5 V, showing good electrochemical stability, which is sufficient to adapt to commercial high-voltage battery systems.[37] To further investigate the influence of PBO flame-retardant additives on the kinetics and long-term cycle stability of LIBs, the rate performance of the LFP/Li half-battery was first tested (Fig. 3d and Table S2 in ESI). The experimental results show that the addition amount of PBO in the liquid electrolyte has a significant impact on its rate response, and the discharge capacity of BE-15% PBO at high rates is even better than that of BE, which is attributed to the excellent lithium-ion transport ability of the PBO oligomer optimized by molecular design. However, when the addition amount was further increased to 20%, owing to the decrease in the effective concentration of lithium salt, the impedance increased, thereby deteriorating the overall electrochemical performance of the liquid electrolyte. In the LFP/Gr coin cell (Fig. 3e), BE-15% PBO demonstrated superior cycle stability compared to that of BE-5% PFPN. At a current density of 0.5 C, both the BE-5% PFPN and BE-15% PBO cells exhibit an initial discharge capacity of approximately 140 mAh·g^{-1}, which is higher than that of the BE cell. After 250 cycles, the capacity retention of the BE-15% PBO cell was 83.9%, which is significantly higher than that of the BE-5% PFPN cell (72.4 %). Even after 300 cycles at 1.0 C (Fig. S3 and Table S3 in ESI), the capacity retention of the BE-15% PBO cell (84.9%) was higher than that of the BE-5% PFPN cell (81.1%), indicating that the PBO flame retardant exhibited better long-cycle stability than PFPN. Although PFPN shows stability in the initial stage owing to the formation of a rich LiF interface layer, its continuous decomposition leads to rapid performance degradation in the long cycle.[38] In contrast, PBO can form a stable LiF-rich interface layer at the interface, thereby continuously suppressing side reactions during long cycles and delaying performance degradation, thus demonstrating superior cycle stability.

This advantage is particularly prominent in 1 Ah commercial pouch batteries (Fig. 3f and Table S4 in ESI). At a current density of 1.0 C, the initial capacity of BE-15% PBO was close to that of BE, and after 200 cycles, its retention was as high as 95.1%, meeting the requirements of commercial high-density charging and discharging. Through the analysis of the charge-discharge curves (Figs. S4 and S5 in ESI), it can be seen that the voltage polarization of BE-5% PFPN increases significantly during the cycle, while the charging and discharging platform voltage difference of BE-15% PBO remains within a reasonable range of 0.2–0.4 V and no obvious overpotential is generated, proving that the evolution of the interface internal resistance is more gentle and the electrochemical stability is stronger.[39]

In terms of graphite anode compatibility, the cyclic voltammetry (CV) curves of the Gr/Li half-cell (Figs. 3g–3i) show that BE-5% PFPN exhibits a weak reduction peak at 0.4–1.2 V, indicating that PFPN preferentially reduces EC to form a rich LiF interface layer; while BE-15% PBO only shows the standard EC reduction and lithium-ion insertion-extraction behavior during the scan, without any additional side reaction peaks. This proves that PBO has excellent compatibility with the graphite anode, avoiding the interface impedance increase and capacity degradation caused by the excessive adsorption of small-molecule flame retardants on the anode surface.[6,40] This was also strongly verified by the EIS tests (Fig. S6 and Table S5 in ESI). At the beginning of the LFP/Gr all-cell cycling, the impedance differences among the various systems were relatively small; however, after 200 cycles, the charge transfer impedance (R_{ct}) of the BE-5% PFPN cell increased dramatically to 48.6 Ω, indicating that the decomposition products of PFPN would lead to interface deterioration during the cycling process. In contrast, the R_{ct} of the BE-15% PBO cell after cycling is only 8.2 Ω, even lower than that of BE, demonstrating that the interface layer constructed by PBO on the electrode surface has excellent stability and ion conductivity.

Overall, the PBO oligomer significantly improved the thermal safety of the liquid electrolyte while maintaining excellent ionic kinetic performance and a broad electrochemical window, demonstrating great potential as an inherently safe liquid electrolyte additive. Compared to previously reported liquid electrolyte additives and the commercial flame-retardant liquid electrolyte additive PFPN, the PBO oligomer additive demonstrated significant advantages in terms of capacity, rate performance, and cycle life, exhibiting outstanding comprehensive performance (Fig. 3j and Table S9 in ESI).

Molecular Dynamics Simulation of Electrolytes

To investigate the influence of PBO oligomers on the coordination and migration ability of lithium ions, the electrostatic potential (ESP) distribution of the model molecule diethyl glycol monoethyl ether phenoxyacetate (DDPP, serving as a model molecule representing the repeating unit of the PBO oligomer) and the commercial reference PFPN, as well as their binding energies with lithium ions, were simulated using density functional theory (DFT) (Figs. 4a and 4b). The results show that the negative region of the ESP of the DDPP molecule (red) is significantly concentrated at the P=O, C−O polar groups and the introduced benzene ring structure, with the most negative value being approximately –47.06 kcal·mol^{-1}, which is much lower than –25.34 kcal·mol^{-1} of PFPN. This indicates that PBO has a stronger electrostatic attraction effect on Li^+, and the calculated binding energy (Figs. 4c and 4d) (–63.57 kcal·mol^{-1} for PBO versus –38.65 kcal·mol^{-1} for PFPN) also confirms that a more stable coordination center is formed between DDPP and Li^+. Additionally, based on frontier orbital theory analysis (Fig. 4e), PBO has the lowest unoccupied molecular orbital (LUMO) energy level, enabling it to preferentially undergo reduction compared to the solvent components.[41,42]

To explore the influence of flame-retardant additives on the solvation shell structure of the electrolyte, molecular dynamics (MD) simulations were conducted on three liquid electrolyte systems: BE, BE-5% PFPN, and BE-15% PBO. In the

https://doi.org/10.1007/s10118-026-3897-x

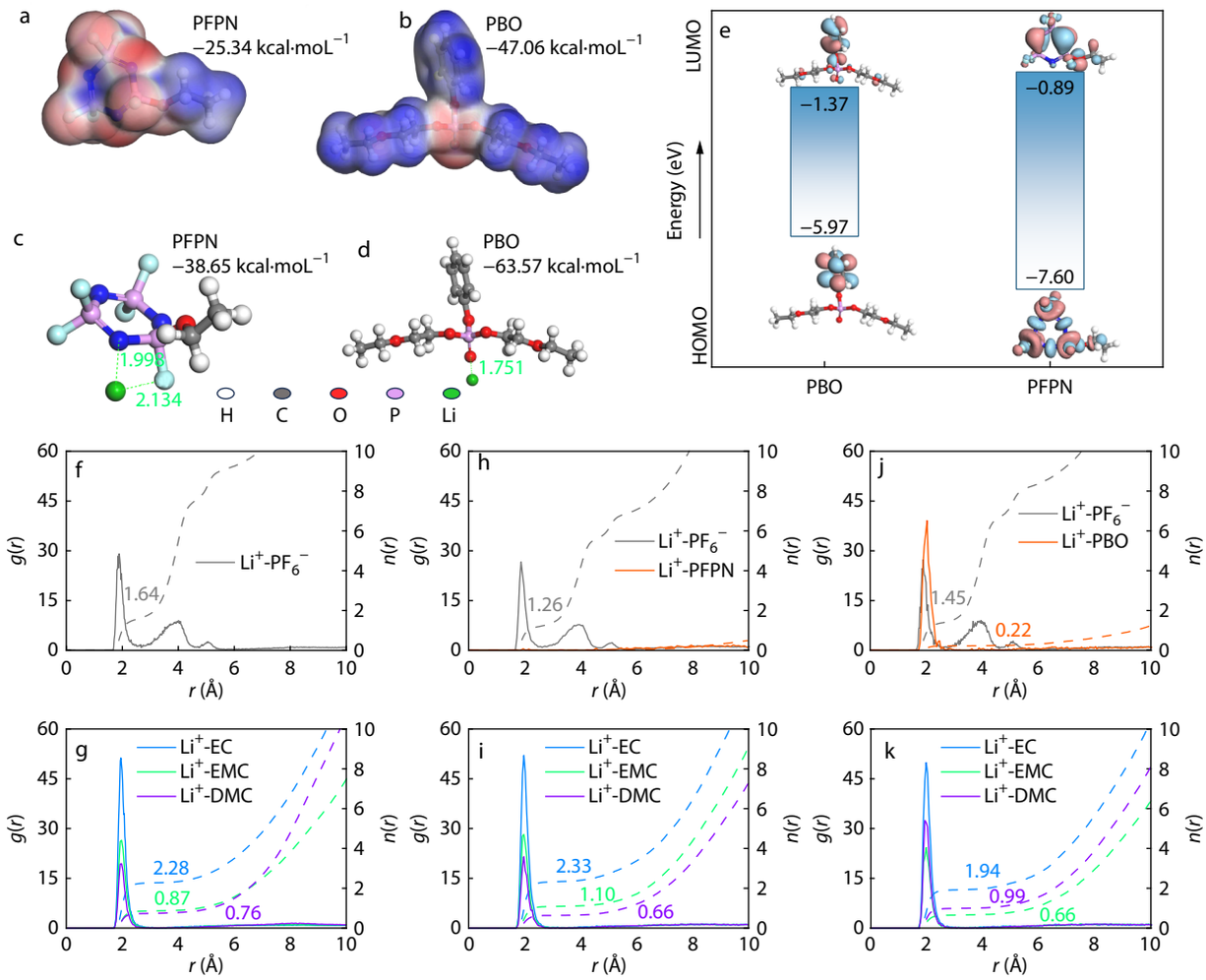


Fig. 4 Molecular electrostatic potential of (a) PFPN and (b) PBO; Lithiophilic sites of (c) PFPN and (d) PBO; (e) HOMO and LUMO levels of PBO and PFPN; The radial distribution functions ($g(r)$, solid lines) and coordination numbers ($n(r)$, dashed lines) of (f, g) BE, (h, i) BE-5% PFPN and (j, k) BE-15% PBO.

BE electrolyte (Figs. 4f and 4g), Li^+ was mainly surrounded by carbonate solvents (especially EC molecules). Owing to the lack of protection by strong coordinating additives, this traditional solvation structure is prone to the continuous reduction and decomposition of solvent molecules on the graphite anode surface.[41] In contrast, in BE-5% PFPN (Figs. 4h and 4i), the coordination distance between Li^+ and the N or P atoms in PFPN was relatively large. This indicates that the interaction between the small molecules PFPN and Li^+ is weak, making it difficult for them to occupy a dominant position in the solvation shell, resulting in more frequent phase decomposition rather than ordered film formation during the cycling process.

As shown in Figs. 4(j) and 4(k), Li^+ exhibited significant coordination with the phosphoryl oxygen (O—P=O) and ether bond oxygen (O—C—O) in the PBO molecule. The characteristic peak of Li^+-O—P=O appears at approximately 1.95 Å, with a significantly higher peak intensity than other components, indicating that the P=O group in the PBO molecule has a very strong ability to capture Li^+. This strong coordination interaction helps the PBO preferentially participate in the construction of the solvation shell. At the same time, the introduction of PBO led to a decrease in the coordination number of Li^+ with the carbonate solvent (EC/EMC), proving that PBO successfully replaced some solvent molecules and formed a protective solvation layer dominated by oligomers, which was conducive to the preferential reduction of film formation at the interface.[43]

Characterization of SEI and CEI

Microscopic morphology observation using scanning electron microscopy (SEM) was conducted to reveal the construction process of the interface layer. On the anode side, the SEM images showed that the surface of the graphite particles was completely covered by a polymer layer with a thickness of approximately 1–2 μm in BE-15% PBO (Figs. 5a and 5b). This layer effectively inhibited the growth of Li dendrites and maintained the integrity of the graphite structure. A schematic of the morphology of the electrolyte/graphite interface on the graphite anode for different liquid electrolytes is shown in Fig. 5(c). The electrolyte/graphite interface for BE-5% PFPN was composed of an unstable SEI, which was easily destroyed by the graphite volume expansion during cycling. In contrast, for BE-15% PBO, a

https://doi.org/10.1007/s10118-026-3897-x

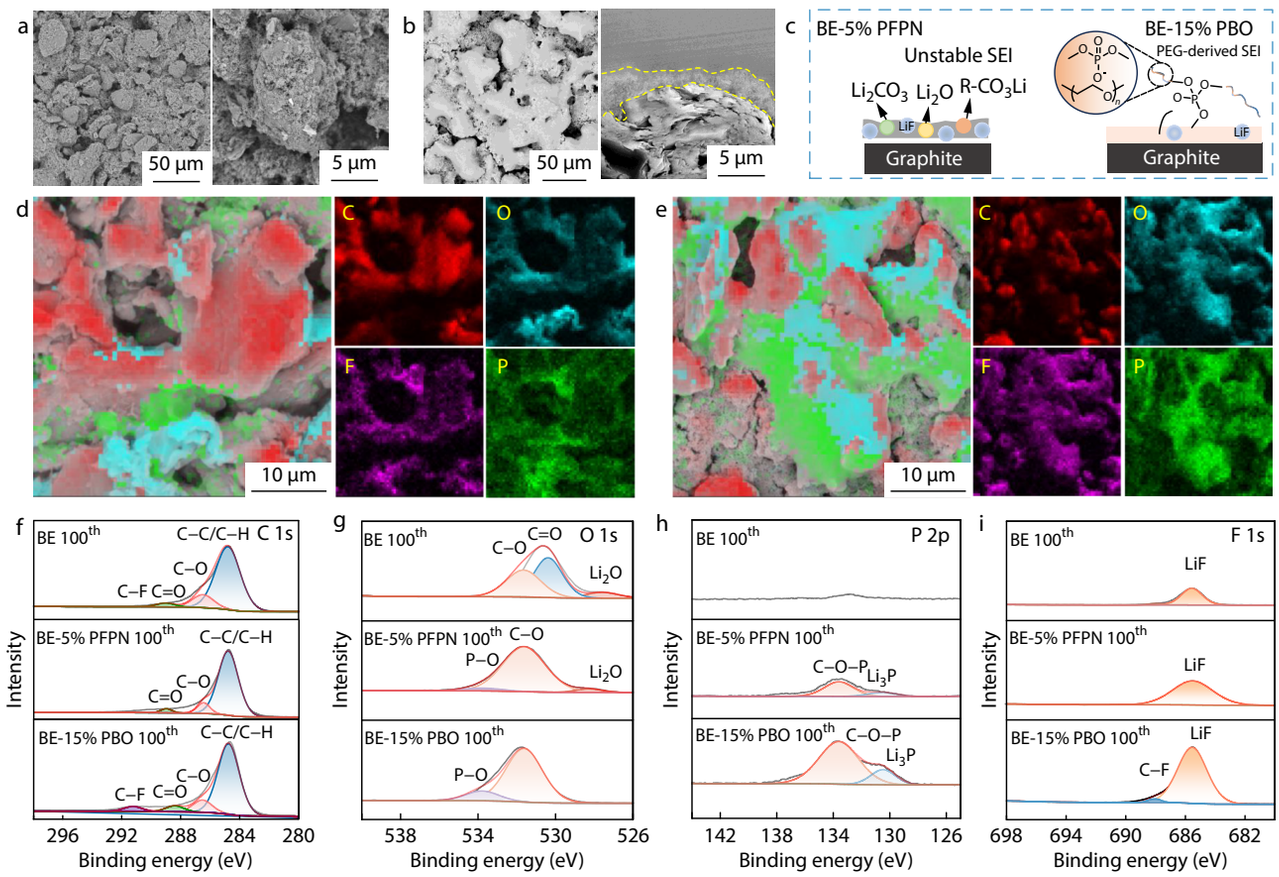


Fig. 5 SEM images of graphite anodes with (a) BE-5% PFPN and (b) BE-15% PBO liquid electrolytes after cycling; (c) Schematic illustration of the interfaces formed with BE-5% PFPN and BE-15% PBO during cycling; Surface element mapping of graphite anodes after 200 cycles with (d) BE-5% PFPN and (e) BE-15% PBO; XPS analysis of (f) C 1s, (g) O 1s, and (h) P 2p and (i) F 1s after 100 cycles of BE, BE-5% PFPN and BE-15% PBO graphite anodes, respectively.

thin polymer electrolyte/graphite interface that spontaneously adapts to the graphite volume expansion to resist cracks and promote Li-ion migration could be formed on the graphite anode, thereby resulting in excellent stability of the BE-15% PBO cells during long-term cycling.

Energy dispersive spectroscopy (EDS) (Figs. 5d, 5e, and Table S6 in ESI) revealed that compared to the SEI on the BE-5% PFPN surface, which is mainly composed of inorganic LiF components, the interface layer formed by BE-15% PBO is rich in phosphorus/oxygen organic components and has a more continuous distribution. At the cathode side, the introduction of the PFPN flame retardant did not significantly alter the overall morphology of the cathode or the morphology of the LFP particles. However, under a higher magnification in the SEM, the surface of the LFP particles in the BE-PBO battery was covered by continuous interface layers. It is speculated that the PBO flame retardant can also form interface layers on the cathode surface (Fig. S7 in ESI), and the EDS energy spectra (Fig. S8 and Table S7 in ESI) show the uniform distribution of P and O, confirming that PBO actively participates in the construction of the cathode/electrolyte interface (CEI).

To reveal the mechanism by which BE-15% PBO enhances the cycling performance at the microscopic level, the surface components of the graphite anode after cycling were analyzed by X-ray photoelectron spectroscopy (XPS). In the C 1s spectra (Fig. 5f), BE-15% PBO exhibited strong C—O and C=O signals. Combined with the characteristic peak at 532.5 eV in the O 1s spectra (Fig. 5g), it was confirmed that the PBO oligomer preferentially underwent electrochemical reduction at the anode surface and formed an SEI film rich in polymer components. Notably, in the P 2p spectra (Fig. 5h), C—O—P (133.8 eV) and Li_3P (130.5 eV) signals were observed, indicating that the phosphorus-containing functional groups in the PBO were successfully integrated into the interface layer. The presence of Li_3P is beneficial because it not only provides fast Li^+ conduction pathways but also serves as a nucleation-inducing site to guide uniform lithium deposition, ultimately endowing the interface layer with superior electrochemical stability and dendrite-suppression capability.[44–46] Furthermore, from the F 1s spectra results (Fig. 5i), it can be observed that BE, BE-5% PFPN, and BE-15% PBO all form interface layers containing LiF. However, BE-15% PBO had a relatively high LiF content, which endowed the interface layer with excellent mechanical properties. This can prevent the continuous decomposition of the liquid electrolyte on the graphite anode surface and the repeated cracking and regeneration of the interface layer, thereby significantly improving long-cycle stability. Compared to brittle inorganic components (such as Li_2CO_3) generated by solvent decomposition in the BE electrolyte, the polymer-based interface layer derived

https://doi.org/10.1007/s10118-026-3897-x

from PBO has better flexibility and structural integrity. Moreover, this phosphorus-rich organic-inorganic composite SEI film has a higher ionic conductivity, optimizing the diffusion dynamics of lithium ions at the interface, thereby achieving long-life and high-rate operation of pouch batteries while ensuring the inherent safety of the liquid electrolyte. Based on the above analysis, PBO as a functional oligomer additive achieves a balance between macroscopic thermal safety improvement and microscopic interface stability, demonstrating electrochemical adaptability beyond traditional small-molecule flame retardants.

Safety Performance of Cells

The battery thermal runaway process consists of three characteristic temperatures: T_1 is the initial temperature ($dT/dt \geq 0.02$ °C·min^{-1}), corresponding to the decomposition of the anode SEI; T_2 is the triggering temperature ($dT/dt \geq 1$ °C·s^{-1}), corresponding to the contraction of the separator causing an internal short circuit; T_3 is the highest temperature, determined by the battery material itself.[47–49] Through accelerated rate calorimetry (ARC) tests on fully charged LFP/Gr batteries, the effects of different additives on the characteristic temperatures of thermal runaway were evaluated (Fig. 6a and Table S8 in ESI). The experimental results show that the self-heating initiation temperatures (T_1) of BE and BE-15% PBO are basically the same, while the T_1 of BE-5% PFPN was earlier. This is mainly attributed to the SEI interphase induced by small-molecule PFPN, which lacks the protective organic-inorganic network found in PBO and contains thermally labile organic decomposition products, leading to early thermal degradation and an earlier T_1 onset. However, during the thermal runaway incubation stage, BE-15% PBO exhibits the most significant inhibitory effect, with an incubation time (Δt) of 1343.6 min, far exceeding BE (446.2 min) and BE-5% PFPN (1020.4 min). This result indicates that the robust phosphorus-containing interface layer formed by PBO on the electrode surface can more effectively prevent exothermic secondary reactions between the electrolyte and electrode, reducing the self-heating rate. The T_2 temperatures of the BE, BE-5% PFPN, and BE-15% PBO batteries were 317.7, 325.7 and 331.5 °C

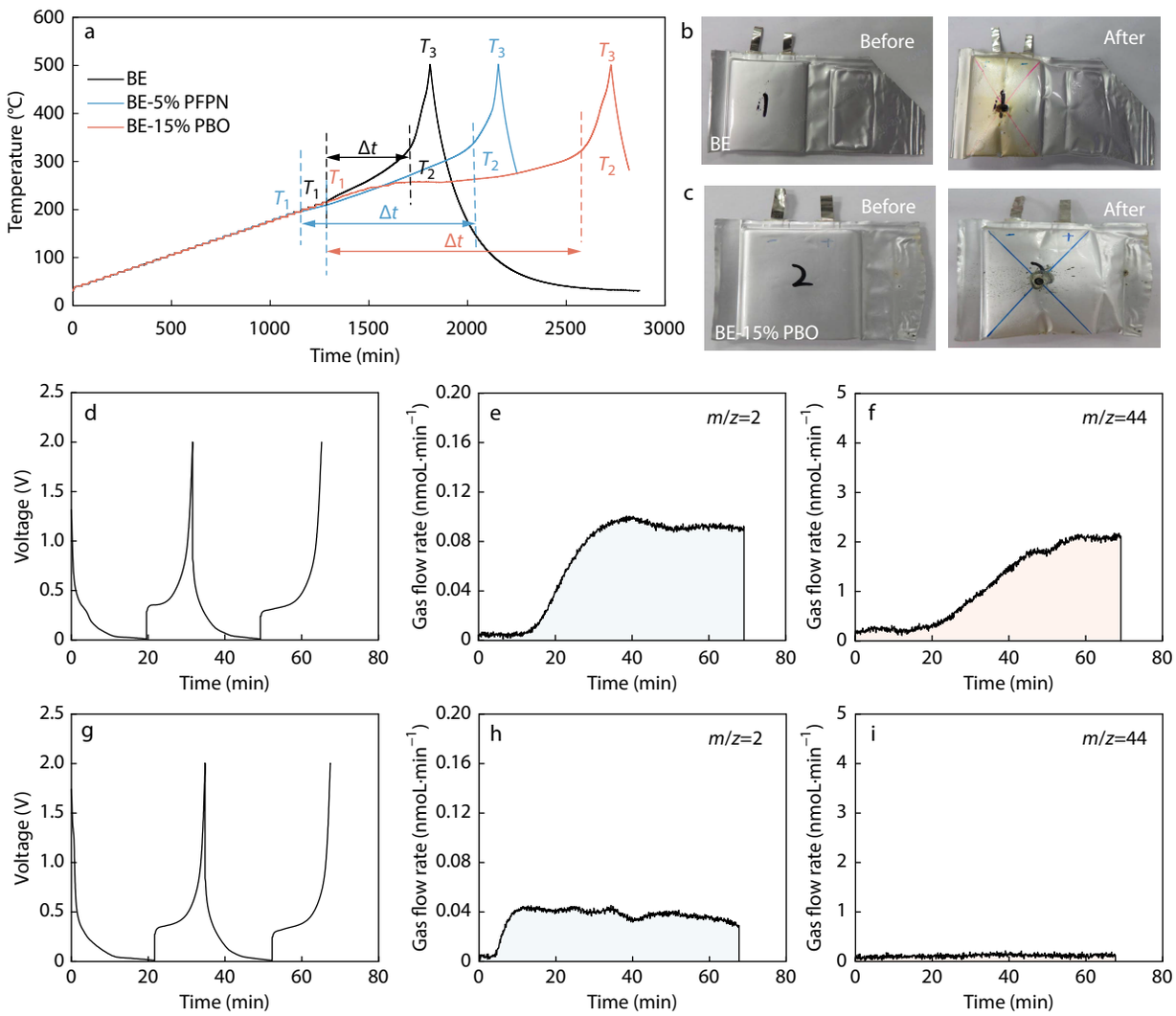


Fig. 6 (a) Temperature and time curves of the cells with different liquid electrolytes in accelerated rate calorimetry tests; Status of pouch cells with (b) BE and (c) BE-15% PBO liquid electrolytes before and after puncturing; DEMS measurements for the Gr/Li cells with (d–f) BE and (g–i) BE-15% PBO.

https://doi.org/10.1007/s10118-026-3897-x

respectively. This indicates that the introduction of flame retardants enabled the batteries to reach the ignition temperature only at higher temperatures, thereby ensuring the fire safety of the liquid electrolyte while also improving the thermal stability of the batteries.

The nail puncture test further verified the protective efficacy of the PBO under abusive conditions. As shown in Fig. 6(b), Figs. S9 and S10 (in ESI), after puncture in the BE battery, due to intense redox reactions, the surface temperatures of the cathode and anode rise rapidly to 272.8 and 249.3 °C, accompanied by a large amount of combustible smoke containing CO, CH_4, and C_2H_4 produced by solvent evaporation and electrolyte decomposition. In contrast, as shown in Fig. 6(c), Figs. S9 and S10 (in ESI), the BE-15% PBO battery not only has a significantly lower peak temperature (cathode and anode, 176.7 and 91.2 °C respectively), but also shows no obvious gas production or structural damage throughout the process. This excellent safety is attributed to the high-quality SEI and CEI layers formed by PBO, which have excellent thermal stability and effectively act as a physical barrier under extreme conditions, inhibiting direct contact between the cathode and anode, as well as chain thermal release.

In situ differential electrochemical mass spectrometry (DEMS) revealed a gas suppression mechanism at the molecular level (Figs. 6d–6i). During the cycling process of the Gr/Li half-cell, the total production of H_2 and CO_2 in the BE (Figs. 6d–6f) is as high as 4.5 and 77.1 nmol respectively, while in the BE-15% PBO (Figs. 6g–6i), it is reduced to 2.4 and 7.7 nmol respectively, with a one-order reduction in gas production rate. The sources of these gases can be summarized as follows: H_2 mainly originates from the reaction of trace moisture in the liquid electrolyte with $LiPF_6$ to form HF, which then reacts with lithium metal, as well as the hydrogen radicals generated when the carbonate solvents (such as EC and DMC) undergo deep reduction on the graphite surface; CO_2 mainly originates from the oxdation reaction of chain-type carbonates (such as DMC and EMC), as well as the chemical or electrochemical decomposition of unstable carbonate components (such as $ROCO_2Li$) in the SEI.[31,50] Combined with the macroscopic performance of the pouch batteries after cycling (Fig. S11 in ESI), the PBO preferentially reduces to a film through its lower LUMO energy level, forming a stable protective layer that fundamentally prevents the continuous decomposition of the electrolyte on the graphite anode surface and the resulting bulging failure. In conclusion, the PBO additive significantly enhanced the inherent safety of the battery in long-term service and extreme abuse conditions through the synergistic effects of thermal inhibition, physical barriers, and chemical passivation.

CONCLUSIONS

This study utilized cost-effective phenoxy phosphorodichloride and PEG as raw materials to synthesize PBO oligomers with efficient flame retardancy and excellent kinetic properties through a one-step process. The application potential of this PBO oligomer as a liquid electrolyte additive in lithium-ion batteries was systematically compared with that of commercial PFPN additives. The results show that PBO, utilizing the high-temperature decomposition mechanism of the phenoxy phosphate group, can achieve efficient self-extinguishing of the liquid electrolyte at a 15% addition level. Moreover, its unique thermal stability and inhibitory effect on solvent evaporation were significantly superior to those of PFPN. In terms of electrochemical performance, the introduction of a benzene ring weakened the interaction between Li^+ and the oxygen of the ether bond, enabling the BE-15% PBO liquid electrolyte to maintain a high ionic conductivity while providing excellent cycle stability (a capacity retention of 95.1% after 200 cycles at 1.0 C) and rate performance for LFP/Gr cells and 1 Ah pouch batteries. This effectively overcame the drawback of the PFPN impedance increase due to the decomposition products. Interface characterization confirmed that PBO could be used to construct a uniform and dense flexible polymer interface layer on the graphite anode surface. This protective layer not only improves the interface dynamics, but also demonstrates significant advantages in delaying the onset time of thermal runaway, reducing the heating rate, and suppressing gas evolution in nail penetration and ARC tests, providing a new idea for enhancing the inherent safety of commercial lithium-ion batteries.

Conflict of Interests

The authors declare no interest conflict.

Electronic Supplementary Information

Electronic supplementary information (ESI) is available free of charge in the online version of this article at http://doi.org/10.1007/s10118-026-3897-x.

Data Availability Statement

The related data of this work can be obtained from the author for reasonable reasons.

ACKNOWLEDGMENTS

This work was financially supported by the National Natural Science Foundation of China (No. U24A6004), Institutional Research Fund from Sichuan University (No. 2021SCUNL201), and State Key Laboratory of Advanced Polymer Materials (No. sklapm2025-2-22).

REFERENCES

1 Wang, Y.; Feng, X.; Huang, W.; He, X.; Wang, L.; Ouyang, M. Challenges and opportunities to mitigate the catastrophic thermal runaway of high-energy batteries. *Adv. Energy Mater.* **2023**, *13*, 2203841.
2 Khan, A.; Al Rashid, H.; Roy, P. K.; Chowdhury, S. I.; Sathi, S. A. Challenges and the way to improve lithium-ion battery technology for next-generation energy storage. *Energy Environ. Mater.* **2025**, *8*, e70088.
3 Chen, G.; Tan, R.; Zeng, C.; Li, Y.; Zou, Z.; Wang, H.; Ouyang, C.; Wan, J.; Yang, J. Developing safe and high-performance lithium-ion batteries: strategies and approaches. *Prog. Mater Sci.* **2025**,

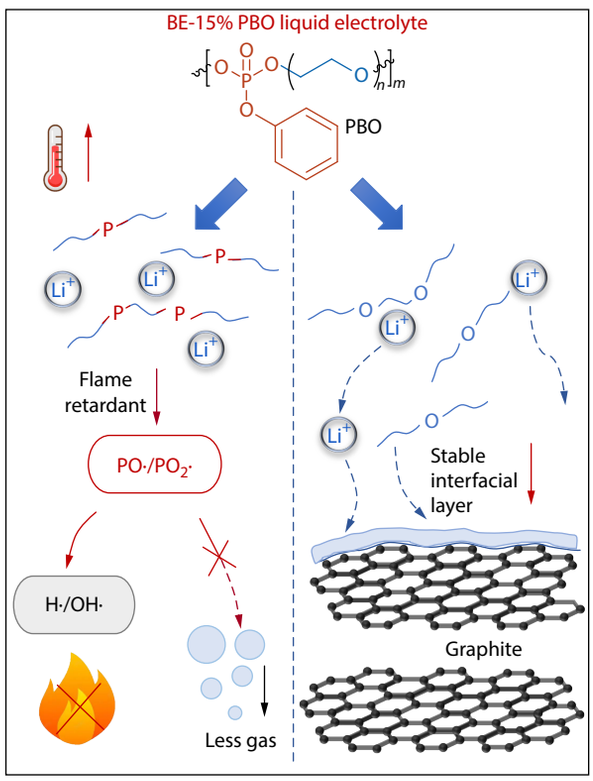
Graphical Abstract

Multifunctional Oligomer as Fluorine-free Flame-retardant Additive of Liquid Electrolytes Enables Simultaneously High Safety and Long-cycle Life in Lithium-ion Batteries

Xing-Di Li, Yi-Zhou Quan, Ji-Yun Ma, and Gang Wu

Sichuan University; Dongfang Electric (Chengdu) Hydrogen Technology Limited

A fluorine-free poly(phenoxyphosphonate-ethylene glycol) oligomer (PBO) additive significantly enhances liquid electrolyte safety by suppressing combustion chain reactions *via* phosphorus-containing radicals and forming a stable interface on graphite anodes. Consequently, 1 Ah pouch cells achieved exceptional 84.6% capacity retention after 250 cycles at 0.5 C with superior thermal runaway resistance.



Chinese J. Polym. Sci. 2026 *https://doi.org/10.1007/s10118-026-3897-x*

154, 101516.

4 Liu, M.; Liu, Q.; Quan, Y.; Yu, J.; Wu, G.; Wang, X. L.; Wang, Y. Z. Phosphorus-silicon-integrated electrolyte additive boosts cycling performance and safety of high-voltage lithium-ion batteries. *Chinese Chem. Lett.* **2024**, *35*, 109123.

5 Cho, W.; Huh, Y. J.; Choi, S.; Kulkarni, U.; Shejale, K. P.; Yi, G. R. Innovations in non-flammable and flame-retardant electrolytes for safer lithium-ion batteries. *Chem. Commun.* **2025**, *61*, 12056–12068.

6 Kim, J. H.; Hyun, J. H.; Kim, S.; Park, W. H.; Yu, S. H. Phosphorus-based flame-retardant electrolytes for lithium batteries. *Adv. Energy Mater.* **2025**, *15*, 2500587.

7 Liu, M. C.; Chen, H. J.; Wu, G.; Wang, X. L.; Wang, Y. Z. Multifunctional robust aerogel separator towards high-temperature, large-rate, long-cycle lithium-ion batteries. *Chinese Chem. Lett.* **2023**, *34*, 107546.

8 Kalhoff, J.; Eshetu, G. G.; Bresser, D.; Passerini, S. Safer electrolytes for lithium-ion batteries: state of the art and perspectives. *ChemSusChem* **2015**, *8*, 2154–2175.

9 Liu, L.; Du, C.; Wang, S.; Chen, S. Three new bifunctional additives for safer nickel-cobalt-aluminum based lithium ion batteries. *Chin. Chem. Lett.* **2018**, *29*, 1781–1784.

10 Cheng, H.; Ma, Z.; Kumar, P.; Liang, H.; Cao, Z.; Xie, H.; Cavallo, L.; Li, Q.; Ming, J. Non-flammable electrolyte mediated by solvation chemistry toward high-voltage lithium-ion batteries. *ACS Energy Lett.* **2024**, *9*, 1604–1616.

11 Jiang, L.; Liang, C.; Li, H.; Wang, Q.; Sun, J. Safer triethyl-phosphate-based electrolyte enables nonflammable and high-temperature endurance for a lithium ion battery. *ACS Appl. Energy Mater.* **2020**, *3*, 1719–1729.

12 Zhang, J.; Li, F.; Yu, L.; Wang, Y.; Wang, K.; Chang, C.; Li, M.; Hao, W.; Qian, X. Research on the explosive characteristics and suppression mechanisms of gas generation during thermal runaway of batteries in a charged state. *Chem. Eng. J.* **2025**, *505*, 159699.

13 Ciosek Högström, K.; Lundgren, H.; Wilken, S.; Zavalis, T. G.; Behm, M.; Edström, K.; Jacobsson, P.; Johansson, P.; Lindbergh, G. Impact of the flame retardant additive triphenyl phosphate (TPP) on the performance of graphite/LiFePO4 cells in high power applications. *J. Power Sources* **2014**, *256*, 430–439.

14 Shi, C.; Wang, M.; Tehrani, Z.; Hong, B.; Wang, M.; Tan, R.; Margadonna, S.; Lai, Y.; Titirici, M. M. Constructing quasi-localized high-concentration solvation structures to stabilize battery interfaces in nonflammable phosphate-based electrolyte. *Adv.*

Sci. **2025**, *12*, 2411826.
15 Mishra, R.; Anne, M.; Das, S.; Chavva, T.; Shelke, M. V.; Pol, V. G. Glory of fire retardants in Li-ion batteries: Could they be intrinsically safer. *Adv. Sustain. Syst.* **2024**, *8*, 2400273.
16 Sheng, Z.; Guo, X.; Gu, R.; Xu, S.; Ma, Y.; Shan, J.; Wei, Z.; Shi, H.; Gong, S.; Xu, J.; Zhang, Y.; Zhu, S.; Qi, G.; Min, Y. A sustained-release strategy of fluorinated solvents enables highly safe lithium metal batteries. *Energy Environ. Sci.* **2025**, *18*, 10238–10249.
17 Zhang, C.; Gu, S.; Zhang, D.; Ma, J.; Zheng, H.; Zheng, M.; Lv, R.; Yu, K.; Wu, J.; Wang, X.; Yang, Q. H.; Kang, F.; Lv, W. Nonflammable, localized high-concentration electrolyte towards a high-safety lithium metal battery. *Energy Storage Mater.* **2022**, *52*, 355–364.
18 Zhu, G. R.; Zhang, Q.; Liu, Q. S.; Bai, Q. Y.; Quan, Y. Z.; Gao, Y.; Wu, G.; Wang, Y. Z. Non-flammable solvent-free liquid polymer electrolyte for lithium metal batteries. *Nat. Commun.* **2023**, *14*, 4617.
19 Qiu, B.; Xie, L.; Liang, K.; Zhu, J.; Zhu, J.; He, C.; Zhang, P.; Mi, H. Improved interfacial compatibility between flame-retardant electrolytes and graphite electrodes by tuning the solvation structure of Li^+. *Appl. Surf. Sci.* **2023**, *612*, 155936.
20 Ding, J.; Yang, C.; Hu, W.; Liu, X.; Zhang, A.; Peng, D.; Han, J.; You, Y. Stabilizing the electrode–electrolyte interface for high-voltage Li||$LiCoO_2$ cells using dual electrolyte additives. *Chem. Sci.* **2025**, *16*, 13723–13730.
21 Wu, W.; Li, T.; Zhao, T.; Qiao, R.; Li, Y.; Chen, S.; Jiang, Z.; Zhang, S.; Mao, C.; Deng, J.; Song, J. Cost-effective interfacial high-concentration electrolyte for stable lithium metal batteries. *Nat. Commun.* **2026**, *17*, 3243.
22 Xie, J.; Lu, Y. C. Designing nonflammable liquid electrolytes for safe li-ion batteries. *Adv. Mater.* **2025**, *37*, 2312451.
23 Long, J.; Huang, J.; Miao, Y.; Huang, H.; Chen, X.; Wu, J.; Li, X.; Chen, Y. A multi-functional electrolyte additive for fast-charging and flame-retardant lithium-ion batteries. *J. Mater. Chem. A* **2024**, *12*, 17306–17314.
24 Chen, Y.; Cao, R.; Liu, Y.; Cheng, T.; He, Z.; Xu, L.; Yu, P.; Jiao, S. Artificial intelligence for the understanding of electrolyte chemistry and electrode interface in lithium battery. *Natl. Sci. Open* **2024**, *3*, 20230039.
25 Dong, L.; Deng, L.; Wang, Z.; Liu, Y.; Zhan, J.; Wang, S.; Fang, Z.; Guo, F.; Liu, C.; Liu, H.; Chen, H. A self fire-extinguishing and high rate lithium-fluorinated carbon battery realized by ethoxy(pentafluoro)cyclotriphosphazene electrolyte additive design. *Nano Energy* **2024**, *131*, 110309.
26 Zhou, Z.; Chen, G.; Yu, G.; Liu, X.; Chou, S. Recent achievements on nonflammable electrolytes with ethoxy(pentafluoro)cyclotriphosphazene for stable and safe lithium-ion batteries. *Chem. Sci.* **2026**, *17*, 14887–14900.
27 Liu, Q. S.; Quan, Y. Z.; Liu, M. C.; Zhu, G. R.; Wang, X. L.; Wu, G.; Wang, Y. Z. Electrode-compatible fluorine-free multifunctional additive regulating solid electrolyte interphase and solvation structure for high-performance lithium-ion batteries. *J. Energy Chem.* **2023**, *83*, 239–246.
28 Long, M.-C.; Wang, T.; Duan, P. H.; Gao, Y.; Wang, X. L.; Wu, G.; Wang, Y. Z. Thermotolerant and fireproof gel polymer electrolyte toward high-performance and safe lithium-ion battery. *J. Energy Chem.* **2022**, *65*, 9–18.
29 Quan, Y. Z.; Liu, Q. S.; Liu, M. C.; Zhu, G. R.; Wu, G.; Wang, X.-L.; Wang, Y.-Z. Flame-retardant oligomeric electrolyte additive for self-extinguishing and highly-stable lithium-ion batteries: Beyond small molecules. *J. Energy Chem.* **2023**, *84*, 374–384.
30 Yadav, V.; Wiebenga, M. H.; Haddad, D.; Salvador, J. R.; Pieczonka, N. P. W.; Schmidt, R. D.; Gonzalez Malabet, H. J.; Wang, L. *In situ* analysis and mechanistic understanding of gas species generated in battery cells during thermal abuse. *J. Energy Chem.* **2026**, *114*, 699–708.
31 Feng, X.; Ouyang, M.; Liu, X.; Lu, L.; Xia, Y.; He, X. Thermal runaway mechanism of lithium ion battery for electric vehicles: a review. *Energy Storage Mater.* **2018**, *10*, 246–267.
32 Yu, M.; Gao, Z.; Xie, W.; Shi, X.; Zhang, O.; Shen, Z.; Fang, L.; Ren, M.; Sun, J. A novel strategy utilizing oxidation states of phosphorus for designing efficient phosphorus-containing flame retardants and its performance in epoxy resins. *Polym. Degrad. Stabil.* **2024**, *230*, 111016.
33 Pesko, D. M.; Jung, Y.; Hasan, A. L.; Webb, M. A.; Coates, G. W.; Miller, T. F.; Balsara, N. P. Effect of monomer structure on ionic conductivity in a systematic set of polyester electrolytes. *Solid State Ionics* **2016**, *289*, 118–124.
34 Torell, L. M.; Angell, C. A. Ion-matrix coupling in polymer electrolytes from relaxation time studies. *Br. Polym. J.* **1988**, *20*, 173–179.
35 Cheon, H. J.; Vu, T. T.; Woo, M.; Kim, Y.; Choi, H.; Kim, J.; Choi, Y.; Kim, Y. A.; Yun, J. W.; Ko, Y.; Chang, M. Dual-functional additive for solid polymer electrolytes for enabling highly safe and long-life all-solid-state lithium metal batteries. *ACS Sustainable Chem. Eng.* **2024**, *12*, 2686–2699.
36 Teherpuria, H.; Mohapatra, S.; Meel, A. K.; Chowdhury, S. S. P.; Kanchi, S.; Jaiswal, P. K.; Mogurampelly, S. Ionic conductivity mechanisms in PEO–$NaPF_6$ electrolytes. *Nanoscale* **2025**, *17*, 21573–21581.
37 Li, X.; Li, W.; Chen, L.; Lu, Y.; Su, Y.; Bao, L.; Wang, J.; Chen, R.; Chen, S.; Wu, F. Ethoxy(pentafluoro)cyclotriphosphazene (PFPN) as a multi-functional flame retardant electrolyte additive for lithium-ion batteries. *J. Power Sources* **2018**, *378*, 707–716.
38 Sadeghi, B. A.; Wölke, C.; Shevchuk, M.; Stan, M.; Minar, J.; Weiling, M.; Krämer, S.; Baghernejad, M.; Nowak, S.; Röschenthaler, G. V.; Grünebaum, M.; Winter, M.; Cekic-Laskovic, I. Impact of phosphazene-based compounds in an electrolyte additive mixture for enhanced safety and performance of NMC811||Si-graphite cell chemistry. *RSC Appl. Interfaces* **2025**, *2*, 1461–1472.
39 An, S. J.; Li, J.; Daniel, C.; Mohanty, D.; Nagpure, S.; Wood, D. L. The state of understanding of the lithium-ion-battery graphite solid electrolyte interphase (SEI) and its relationship to formation cycling. *Carbon* **2016**, *105*, 52–76.
40 Wang, G.; Wu, Z. S. Electrolyte engineering for a thermally and electrochemically stable interphase on 4.6 V $LiCoO_2$ at 45 °C. *Natl. Sci. Open* **2025**, *4*, 20250041.
41 Chen, X.; Yao, N.; Zeng, B. S.; Zhang, Q. Ion–solvent chemistry in lithium battery electrolytes: From mono-solvent to multi-solvent complexes. *Fundam. Res.* **2021**, *1*, 393–398.
42 Lan, X.; Yang, S.; Meng, T.; Zhang, C.; Hu, X. A multifunctional electrolyte additive with solvation structure regulation and electrode/electrolyte interface manipulation enabling high-performance Li-ion batteries in wide temperature range. *Adv. Energy Mater.* **2023**, *13*, 2203449.
43 Liu, M.; Zeng, Z.; Gu, C.; Ma, F.; Wu, Y.; Wu, Q.; Yang, X.; Chen, X.; Cheng, S.; Xie, J. Ethylene carbonate regulated solvation of triethyl phosphate to enable high-conductivity, nonflammable, and graphite compatible electrolyte. *ACS Energy Lett.* **2024**, *9*, 136–144.
44 Huang, Y.; Wang, C.; Lv, H.; Xie, Y.; Zhou, S.; Ye, Y.; Zhou, E.; Zhu, T.; Xie, H.; Jiang, W.; Wu, X.; Kong, X.; Jin, H.; Ji, H. Bifunctional Interphase Promotes Li^+ De-Solvation and Transportation Enabling Fast-Charging Graphite Anode at Low Temperature.

Adv. Mater. **2024**, *36*, 2308675.
45 Wang, J.; He, K.; Li, S.; Sun, Z.; Yin, Z.; Miao, K.; Li, Y.; Ma, C.; Zhou, J. Charge Delocalization Electrolyte Design to Construct Fast Dynamic Interface for High-Voltage Lithium Metal Batteries. *Adv. Funct. Mater.* **2026**, *36*, e31823.
46 Tu, S.; Zhang, B.; Zhang, Y.; Chen, Z.; Wang, X.; Zhan, R.; Ou, Y.; Wang, W.; Liu, X.; Duan, X.; Wang, L.; Sun, Y. Fast-charging capability of graphite-based lithium-ion batteries enabled by Li3P-based crystalline solid–electrolyte interphase. *Nat. Energy* **2023**, *8*, 1365–1374.
47 Liang, C.; Lai, X.; Shen, K.; Zheng, Y.; Xu, C.; Peng, Y.; Li, J.; Wang, X.; Wang, Y.; Hong, Y.; Ben-Marzouk, M.; Feng, X.; Ouyang, M. Experimental study on immersion cooling for delaying thermal runaway propagation in lithium-ion battery modules. *Process Saf. Environ. Prot.* **2026**, *206*, 108333.
48 Yang, Y.; Wang, R.; Shen, Z.; Yu, Q.; Xiong, R.; Shen, W. Towards a safer lithium-ion batteries: a critical review on cause, characteristics, warning and disposal strategy for thermal runaway. *Adv. Appl. Energy* **2023**, *11*, 100146.
49 Feng, X.; Ren, D.; He, X.; Ouyang, M. Mitigating thermal runaway of lithium-ion batteries. *Joule* **2020**, *4*, 743–770.
50 Wang, Q.; Mao, B.; Stoliarov, S. I.; Sun, J. A review of lithium ion battery failure mechanisms and fire prevention strategies. *Prog. Energy Combust. Sci.* **2019**, *73*, 95–131.

https://doi.org/10.1007/s10118-026-3897-x